





RESEARCH ARTICLE OPEN ACCESS

# Optical Constants and Electron Inelastic Mean-Free Paths of SiO<sub>2</sub>, HfO<sub>2</sub> and CaF<sub>2</sub> Extracted From Reflection Electron Energy Loss Spectra

Wolfgang S. M. Werner<sup>1</sup> 📵 | Vytautas Astašauskas<sup>1</sup> 📵 | Olga Ridzel<sup>2</sup> 📵 | Alessandra Bellissimo<sup>3</sup> 📵 | Michael Stöger-Pollach<sup>4</sup> 📵

<sup>1</sup>Institut für Angewandte Physik, Technische Universität Wien, Vienna, Austria | <sup>2</sup>Theiss Research, La Jolla, California, USA | <sup>3</sup>Institut für Photonik, Technische Universität Wien, Vienna, Austria | <sup>4</sup>Institut für Festkörperphysik, Technische Universität Wien, Vienna, Austria

Correspondence: Wolfgang S. M. Werner (werner@iap.tuwien.ac.at)

Received: 28 September 2024 | Revised: 10 February 2025 | Accepted: 13 March 2025

Keywords: energy loss function | inelastic mean-free path | inorganic insulators | optical constants | reflection electron energy loss spectroscopy

### **ABSTRACT**

Reflection electron energy loss spectroscopy (REELS) spectra were measured for three inorganic compounds ( $SiO_2$ ,  $HfO_2$  and  $CaF_2$ ). VIS-XUV optical constants were extracted from the measured REELS spectra after elimination of multiple inelastic scattering by deconvolution. The derived normalised single scattering loss distributions were fitted to a Drude-type dielectric function. The resulting optical constants reasonably satisfy the Kramers–Kronig and f-sum rules. Values for the energy band gap were also determined from the deconvoluted loss spectra. Special attention is paid to the extension of the optical constants onto the complex plane and its relation to the kinematics in an inelastic collision for a material with a given electronic structure. The analysis suggests differences in the elementary scattering kinematics in a REELS experiment between insulators and metals. Describing the dispersion of the loss features on the complex plane by the dispersion constant  $\alpha$ , we find that the dispersion constant  $\alpha$  in the analysis of REELS data should be treated as a fit parameter or, alternatively, use of a vanishing value for insulators and  $\alpha = 1$  for conductors is recommended. For evaluating the inelastic mean-free path (IMFP) from optical constants,  $\alpha$  should always be taken to be unity.

### 1 | Introduction

Inorganic insulating materials, such as those used in the present study, that is, hafnium oxide (HfO $_2$ ), calcium fluoride (CaF $_2$ ) and silicon dioxide (SiO $_2$ ), have a wide range of applications in science and technology. Hafnium dioxide (HfO $_2$ ) is one of the mature high-k dielectrics in the microelectronics industry as it is an alternative to SiO $_2$  [1]. Calcium fluoride (CaF $_2$ ) is one of the most widely used thermoluminescent detectors in environmental monitoring, medical and space dosimetry [2, 3] and is also used as an optical component because of its chemical stability under adverse conditions [4].

Electron energy loss spectroscopy in reflection mode (Reflection electron energy loss spectroscopy [REELS]) has been employed

by many authors to derive the dielectric function  $\epsilon(\omega,q)$  of a material, where  $\omega$  and q represent the energy loss and the momentum transfer in an interaction. While REELS measurements are experimentally the most simple means to determine VIS-XUV optical constants of solids, there exists some confusion in the literature regarding the quantitative interpretation of the raw data. Since REELS spectra contain contributions of multiple scattering in the volume of the materials as well as surface excitations occurring during the penetration of the surface, the first step is to deconvolute multiple scattering [5, 6]. Then, the resulting single scattering loss distributions are fitted to a model dielectric function modelled through a series of oscillators with a given resonance frequency  $\omega_i$ , damping coefficient  $\gamma_i$ , and amplitude  $A_i$ . Here, an assumption needs to be made concerning the dispersion, that is, the dependence of each oscillator with

This is an open access article under the terms of the Creative Commons Attribution License, which permits use, distribution and reproduction in any medium, provided the original work is properly cited.

© 2025 The Author(s). Surface and Interface Analysis published by John Wiley & Sons Ltd.

resonance frequency (energy)  $\omega$  on the momentum transfer q, which is generally unknown. The following approximation is usually used:

$$\omega_i(q) = \omega_i(q=0) + \alpha q^2/2 \tag{1}$$

The choice of  $\alpha = 1$  is generally made when studying free electron materials, whereas a value close to zero is often used for flat band materials or insulators [7]. Alternatively, the value of  $\alpha$  is also varied in the fitting procedure, together with the values for the resonance frequencies, oscillator strengths and damping parameters. While it has been stated in the literature [7] that the above choices for  $\alpha$  are justified by the electronic structure of the involved materials, it is not clear how and why the dispersion of the energy bands in a solid are related to the dispersion of the loss features, such as a plasmon [8]. Furthermore, for sufficiently large values of the momentum transfer q, energy conservation requires any loss feature to merge into the Bethe-ridge, corresponding to  $\alpha = 1$ . Indeed, Vos [9] has shown in the case of  $TiO_2$ , that for large *q*-values, the Mermin-dielectric function, which inherently assumes a quadratic dispersion ( $\alpha = 1$ ), describes the electron scattering Compton profile (the momentum profile across the Bethe-ridge) very accurately. Thus, for the evaluation of inelastic scattering parameters, such as the IMFP, a value of  $\alpha = 1$  should always be used (as, e.g., in Reference [10]). These considerations imply that the parameter  $\alpha$  used in the fitting procedure of REELS cannot generally be identified with the plasmon dispersion.

A quadratic plasmon dispersion (corresponding to  $\alpha=1$ ) has been experimentally verified for PMMA by energy loss measurements in transmission as a function of the momentum transfer in a transmission electron microscope. On the other hand, in our earlier work [11], which included derivation of optical constants for PMMA from reflection electron energy loss spectra, only the choice ( $\alpha \sim 0$ ) gave realistic results for the fitting procedure, while for calculation of the IMFP comparison with elastic peak electron spectroscopy (EPES) exhibited differences of up to a factor of 2 [8]. This comparison is deemed to be decisive since for EPES measurements, the only input parameter in the analysis is the elastic scattering cross-section; no elements of linear response theory whatsoever are required.

In the present paper, an attempt is made to shed further light on the above questions in the analysis of loss spectra of  $HfO_2$ ,  $CaF_2$  and  $SiO_2$  to yield the VIS-XUV optical constants. It is indeed found that a value of  $\alpha$  used in the fitting procedure close to zero is consistent with the choice of the dielectric function and the measured data. On the other hand, in evaluating, for example, the IMFP on the basis of the retrieved optical constants, one should use  $\alpha=1$ . A similar observation has been made earlier for organic insulators [12].

### 2 | Experimental

The surfaces of  $SiO_2$  consisted of a 100-nm-thick amorphous film thermally grown on an amorphous Si-substrate (see also Reference [13]), whereas the layers of  $HfO_2$  were grown by

atomic layer deposition on a Si-substrate. The surface of the CaF $_2$  sample was freshly cleaved using a razor prior to its insertion into the UHV-chamber and subsequently annealed over night at a temperature of 500°C. Samples were inserted into the UHV-chamber (base pressure  $\sim 2\times 10^{-10}$  mbar), and surface cleanliness was monitored by means of X-ray Photoelectron as well as Auger-Meitner Electron Spectroscopy (XPS & AMES). A series of REELS measurements was acquired on each sample for bulk- and surface-sensitive conditions, in order to disentangle the contribution of surface and volume excitations in the analysis. The kinematical conditions in a REELS experiment can be varied either by changing the primary energy (E $_0$ ) of the incident beam or by changing the incidence and emission angles.

Energy loss spectra on the  $\mathrm{SiO}_2$ -surface were measured in a Thermofisher Microlab 310F instrument equipped with a hemispherical mirror analyser (HMA) operated at a pass energy of 20 eV in constant analyser energy mode, resulting in a constant energy resolution of 0.5 eV [14]. The bulk-sensitive REELS spectra from the  $\mathrm{SiO}_2$  surface were acquired by bombarding the target with 3000 eV-primary electrons and with the sample being in the flat position (incidence angle  $0^\circ$ , detection angle  $60^\circ$  with respect to the surface normal). The second more surface sensitive measurement used a primary energy of 500 eV, the angle of incidence was  $20^\circ$ , while the detection angle was  $80^\circ$  relative to the surface normal.

REELS spectra of HfO<sub>2</sub> and CaF<sub>2</sub> were measured in a modified VG ESCALAB MkII spectrometer equipped with a hemispherical mirror analyser (HMA) with a sector angle of 150°, operated at a pass energy of 20 eV. In this instrument, a Kimball Physics ELG-2 electron gun was used as electron source, defocussed to a spot size of about 1 mm in order to minimise radiation damage and surface charging and to suppress diffraction effects in the case of the single crystalline sample of CaF<sub>2</sub>. While surface charging of a few volts occurs for all three samples (monitored using a Time of Flight spectrometer in our experiment), this merely leads to a corresponding slight change of the landing energy and the escape energy which does not affect the results (as explained in detail in Reference [11]). The bulk-sensitive measurement was carried out with 1600 eV-primary electrons (incidence and emission angles both 60° relative to the surface normal); 500 eV-primary electrons were used for the more surface-sensitive measurement (incidence and emission angles of 40° and 80°, respectively).

The dispersion curves for PMMA were measured directly, employing EELS in a transmission electron microscope (TEM). For this purpose, we used a FEI TECNAI G20 TEM equipped with a GATAN GIF2001 energy filter. The TEM was operated in diffraction mode, and thus, access to *q*-space is given directly. The diffraction pattern was shifted across the spectrometer entrance aperture, and a set of 10 data points were recorded within 2Å<sup>-1</sup> for PMMA. The sample was cooled with liquid nitrogen in order to reduce knock-on damage caused by the electron bombardment, Additionally, low-dose conditions were chosen. The beam energy was set to 200 keV, since lower beam energies would have increased radiolysis tremendously. Aluminium is not beam sensitive at all at 200 keV; thus, cooling and low-dose conditions were not employed.

## 3 | Data Analysis

Optical data, in particular in the VIS-XUV regime, are important physical parameters to quantitatively describe the interaction of charged particle beams with solid matter. Measurement of the dielectric function can be performed employing different techniques. Among the most frequently used techniques are optical reflection or absorption measurements [15-18] and electron energy loss measurements, either in transmission [19] or in reflection [6, 20, 21]. Each of these techniques has its advantages and drawbacks, both with respect to the involved experimental challenges as well as data interpretation. The main difference concerns the dependence of the dielectric function  $\varepsilon(\omega,q)$ on the momentum q. In the case of optical measurements, the probing particles carry no significant momentum since the rest mass of the photon is zero, giving the optical dielectric function  $\varepsilon(\omega, q=0)$ . In the transmission electron microscope, the momentum transfer imparted by the probing electron to the solid can be sensitively monitored by varying the detection angle. In a reflection experiment, the situation is more complicated: A large momentum transfer is required to reverse the direction of the incoming electrons, which is provided by an elastic scattering process, where the mass of the interaction partner (the ionic cores in the solid) greatly exceeds the mass of the incoming electrons. An inelastic interaction with the solid state electrons, having a mass comparable to the probing particle, cannot provide a momentum transfer with the required magnitude to effect a direction reversal. Therefore, the momentum transfer in the inelastic processes, q, measured in a reflection energy loss measurement cannot generally be inferred from the experimental conditions.

Such measurements are assumed to comprise all different kinematically possible values of q.

The pair of raw electron energy loss spectra  $y_{1,2}(\omega)$  of all samples is shown in Figure 1, along with the electron spectra after application of the deconvolution procedure described in References [5, 21, 25] and the extraction of the characteristic surface and bulk excitation components, the differential surface excitation probability (DSEP,  $w_s(\omega)$ ) and differential inverse inelastic mean-free path (DIIMFP,  $w_b(\omega)$ ). The first step is equivalent to the Tougaard–Chorkendorff algorithm, yielding the spectra  $y_{1,2}^*(\omega)$  (shown in the middle panels) which consist of a linear combination of the single scattering loss distributions for volume (DIIMFP) and surface scattering (DSEP), as well as a mixed term. The normalised DIIMFP can then be obtained to first-order by the following simple algorithm [5]:

$$w_b(\omega) = u_{01} y_1^*(\omega) + u_{10} y_2^*(\omega) + u_{11} y_1 \otimes y_2^*(\omega)$$
 (2)

where the symbol " $\otimes$ " denotes a convolution over the energy loss and the coefficients  $u_{xy}$  are a function of the partial intensities for surface and bulk scattering. The same formula (with different coefficients) is used to retrieve the DSEP.

The values of the band gap  $E_{\rm g}$  were determined from the onsets of the normalised DIIMFPs by means of a linear fit of the onset of energy losses (red lines in Figure 2). The resulting values of  $E_{\rm g}$  are given in Table 1.

The DIIMFP is related to the dielectric function as follows [28]:

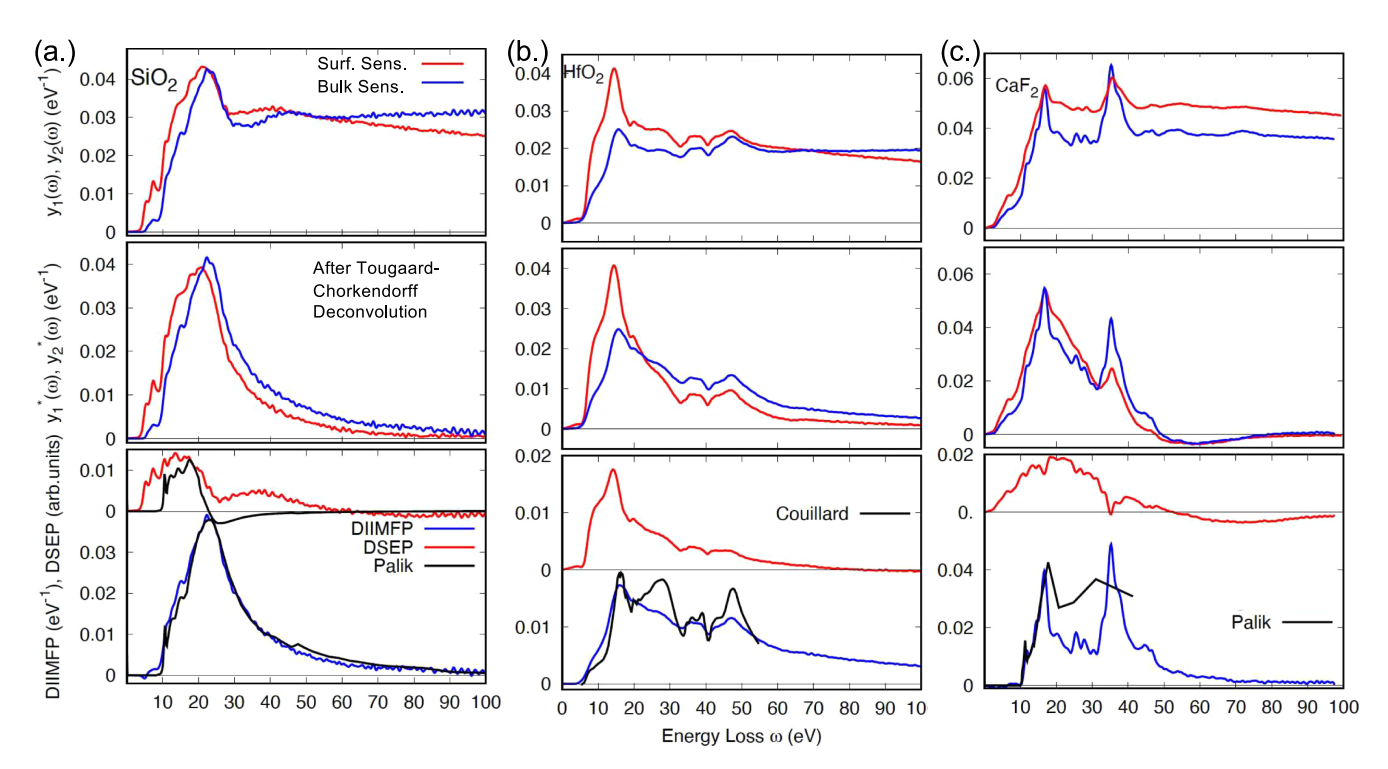


**FIGURE 1** Upper panels: raw energy loss spectra  $y_{1,2}(\omega)$  (after removal of the elastic peak) in absolute units of reciprocal eV for the surface-sensitive measurement (red) and the bulk-sensitive measurement (blue); middle panels: energy loss spectra  $y_{1,2}^*(\omega)$  after application of the Tougaard-Chorkendorff deconvolution [6]; lower panels: normalised DIIMFP in absolute units of reciprocal eV (blue) and DSEP in arbitrary units (red), compared with the energy loss loss function (ELF) (Im{ -1/ $\epsilon(\omega,0)$ }) as found in the literature, represented by the black curves (scaled by a factor facilitating comparison); (a) SiO<sub>2</sub>; black curve: Palik [22]. (b) HfO<sub>2</sub>; black curve: Couillard et al. [23]. (c.) CaF<sub>2</sub>; black curve: Palik [24].

$$W_{b}(\omega, E_{0}) = \int_{q_{-}}^{q_{+}} \frac{d^{2} \lambda^{-1}}{d\omega dq} dq = \frac{\left(1 + E'/c^{2}\right)^{2}}{1 + E'/2c^{2}} \frac{1}{\pi E'} \int_{q_{-}}^{q_{+}} \operatorname{Im}\left[\frac{-1}{\epsilon(\omega, q)}\right] \frac{dq}{q}$$
(3)

where  $\lambda$  is the inelastic mean-free path (IMFP), Im  $\left[-1/\epsilon(\omega,q)\right]$  is the energy loss function (ELF) and  $E'=E_0-E_g$  and integration limits are given by the following:

$$q_{\pm} = \sqrt{E' \left(2 + E'/c^2\right)} \pm \sqrt{\left(E' - \omega\right) \left[2 + \left(E' - \omega\right)/c^2\right]} \quad (4)$$

Here and below atomic units are used ( $\hbar = e = m_e = 1$ ). Note that the lower panels of Figure 1 compare two distinctly different physical quantities: the normalised DIIMFP (Equation (3),

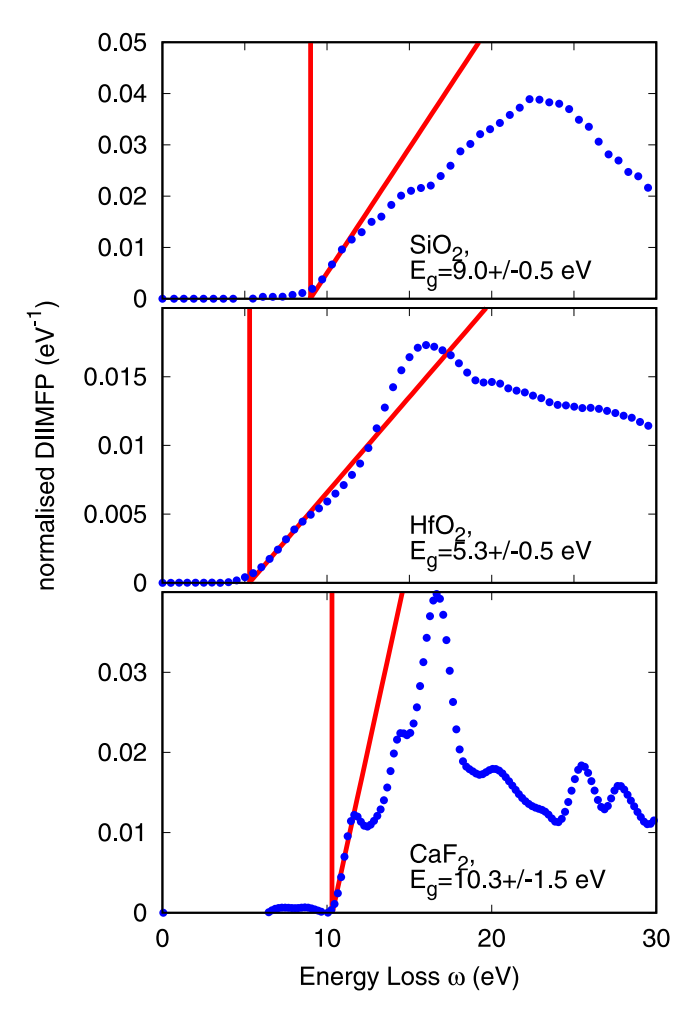


**FIGURE 2** | Normalised differential inverse inelastic mean-free path (DIIMFP) for  ${\rm SiO}_2$ ,  ${\rm HfO}_2$  and  ${\rm CaF}_2$ , illustrating the method to determine the band gap (see text).

blue curves) and the energy loss function  $\text{Im}\left[-1/\epsilon(\omega,q)\right]$  (black curves, scaled to facilitate comparison), appearing in the integrand of Equation (3).

In the present work, the complex dielectric function  $\epsilon(\omega,q)=\epsilon_1+\mathrm{i}\epsilon_2$  is modelled as a sum of Drude oscillators with amplitudes  $A_i$ , binding energies  $\omega_i$  and damping parameters  $\Gamma_i$ :

$$\epsilon_1 = \epsilon_b - \sum_i \frac{A_i \left(\omega^2 - \omega_i(q)^2\right)}{\left(\omega^2 - \omega_i(q)^2\right)^2 + \Gamma_i^2 \omega^2}$$

$$\epsilon_2 = \sum_i \frac{A_i \Gamma_i \omega}{\left(\omega^2 - \omega_i(q)^2\right)^2 + \Gamma_i^2 \omega^2} \tag{5}$$

where  $\epsilon_b$  denotes the background dielectric constant due to the polarizability of the core electrons [31].

The optical constants represented by the oscillator parameters  $A_i$ ,  $\omega_i$ ,  $\Gamma_i$  of the three inorganic compounds were extracted from the normalised DIIMFPs using the approach described in Reference [21]. Optimum values of the oscillator parameters  $A_i$ ,  $\omega_i$ ,  $\Gamma_i$  are found by fitting the NDIIMFP to Equation (3) using the nonlinear optimisation library NLopt [32]. First, a global optimum was obtained employing the augmented Lagrangian algorithm [33, 34] which was then used as a starting point for a local optimization to improve the optimum to a greater accuracy employing the COBYLA (Constrained Optimization BY Linear Approximations) algorithm [35]. Consistency checks were performed employing the Bethe f-sum and Kramers–Kronig or KK-sum rules. The f-sum rule can be evaluated by the following:

$$Z_{\text{eff}} = \frac{1}{2\pi^2 n_a} \int_{E_g}^{\omega_{\text{max}}} \omega \text{Im} \left[ \frac{-1}{\epsilon(\omega, q = 0)} \right] d\omega$$
 (6)

where  $n_a = \frac{N_a \rho}{M}$  is the atomic density,  $N_a$  is Avogadro's number,  $\rho$  is the mass density and M is the molecular weight. At the maximum energy loss  $\omega_{\max} \to \infty$ , the value of  $Z_{\rm eff}$  must approach the atomic number Z. The Kramers–Kronig sum or KK-sum is evaluated as follows:

$$P_{\text{eff}} = \frac{2}{\pi} \int_{E_g}^{\omega_{\text{max}}} \frac{1}{\omega} \text{Im} \left[ \frac{-1}{\epsilon(\omega, q = 0)} \right] d\omega + \frac{1}{n(0)^2}$$
 (7)

where n(0) is the limiting value of the refractive index at low photon energies [28]. At  $\omega_{\rm max} \to \infty$ , the value of  $P_{\rm eff}$  must approach 1. The physical quantities used in Equations (6) and (7) are listed in Table 1.

**TABLE 1** | Material parameters used in this study: molecular weight M, number of valence electrons per molecule  $N_v$ , mass density  $\rho$ , atomic density  $n_a$ , static refractive index n(0), band gap  $E_g$ , width of the valence band  $E_{vb}$ , free-electron plasmon energy  $E_p$ .

Compound	M	$N_{ u}$	$\rho\left(\mathbf{g}\cdot\mathbf{cm}^{-3}\right)$	$n_a(\mathring{A}^{-3})$	<b>n</b> (0)	$E_{\rm g}$ (eV)	$E_{vb}$ (eV)	$E_p$ (eV)
SiO <sub>2</sub>	60.085 [26]	16 [ <b>27</b> ]	2.19 [26]	0.065	1.4585	$9.0 \pm 0.5$	10 [28]	22.0
$\mathrm{HfO}_2$	210.49 [26]	16 [ <b>27</b> ]	9.68 [26]	0.083	1.89 [29]	$5.3 \pm 0.5$	6.5	24.7
CaF <sub>2</sub>	78.075 [26]	16 [ <b>27</b> ]	3.18 [26]	0.073	2.61 [24]	$10.3 \pm 1.5$	5.84 [30]	23.2

The IMFP  $\lambda$  for an electron energy  $E_0 > E_g + E_{vb}$  measured from the bottom of the valence band is then determined by integrating the DIIMFP given by Equation (3) over the energy loss  $\omega$  as follows:

$$\lambda_{in}^{-1}\big(E_0\big) = \int\limits_{E_g}^{E_0-E_g-E_{\rm vb}} W_b\big(\omega,E_0\big)d\omega \tag{8}$$

where  $E_{\rm vb}$  is the width of the valence band.

### 4 | Results and Discussion

The method to deconvolute a pair of loss spectra taken at different kinematical conditions is shown in Figure 1. The upper panels are the raw data which have been subjected to a Lucy–Richardson deconvolution [36]; the elastic peak was fitted to a Gaussian and the intensities were brought on an absolute scale of reciprocal eV by division with the elastic peak area [5]. The red and blue curves show the results for the surface- and bulk-sensitive conditions, respectively. The middle panels are the results of the Tougaard–Chorkendorff procedure [6]. In all cases, higher intensity is seen for

the surface-sensitive spectra at low energy losses (below  $\sim$ 10 eV), demonstrating the fact that these spectra consist of contributions due to surface and bulk excitations as well as a mixed term [5]. The lower panels are the resulting normalised DIIMFP and DSEP. The comparison of the DIIMFP with available literature data (represented by the black curves) is satisfactory; for CaF $_2$ , literature data in the UV regime are sparse.

Determination of the band gap from the REELS spectra is illustrated in Figure 2, and the resulting band gap values are also shown in Table 1.

Figure 3 shows the fit of the normalised DIIMFP extracted from the REELS spectra to the normalised DIIMFP calculated using Equation (3) based on the Drude model dielectric function (Equation 5). A value of  $\alpha=0.1$  in Equation (1) was assumed for each compound. Table 2 shows the f-sum and KK-sum errors for the studied inorganic compounds demonstrating acceptably small discrepancy with the errors less than 10%. The resulting oscillator parameters optimally fitting the experimental data on a model Drude dielectric function are presented in Table 3. The similarity of the present data for the normalised DIIMFP (blue

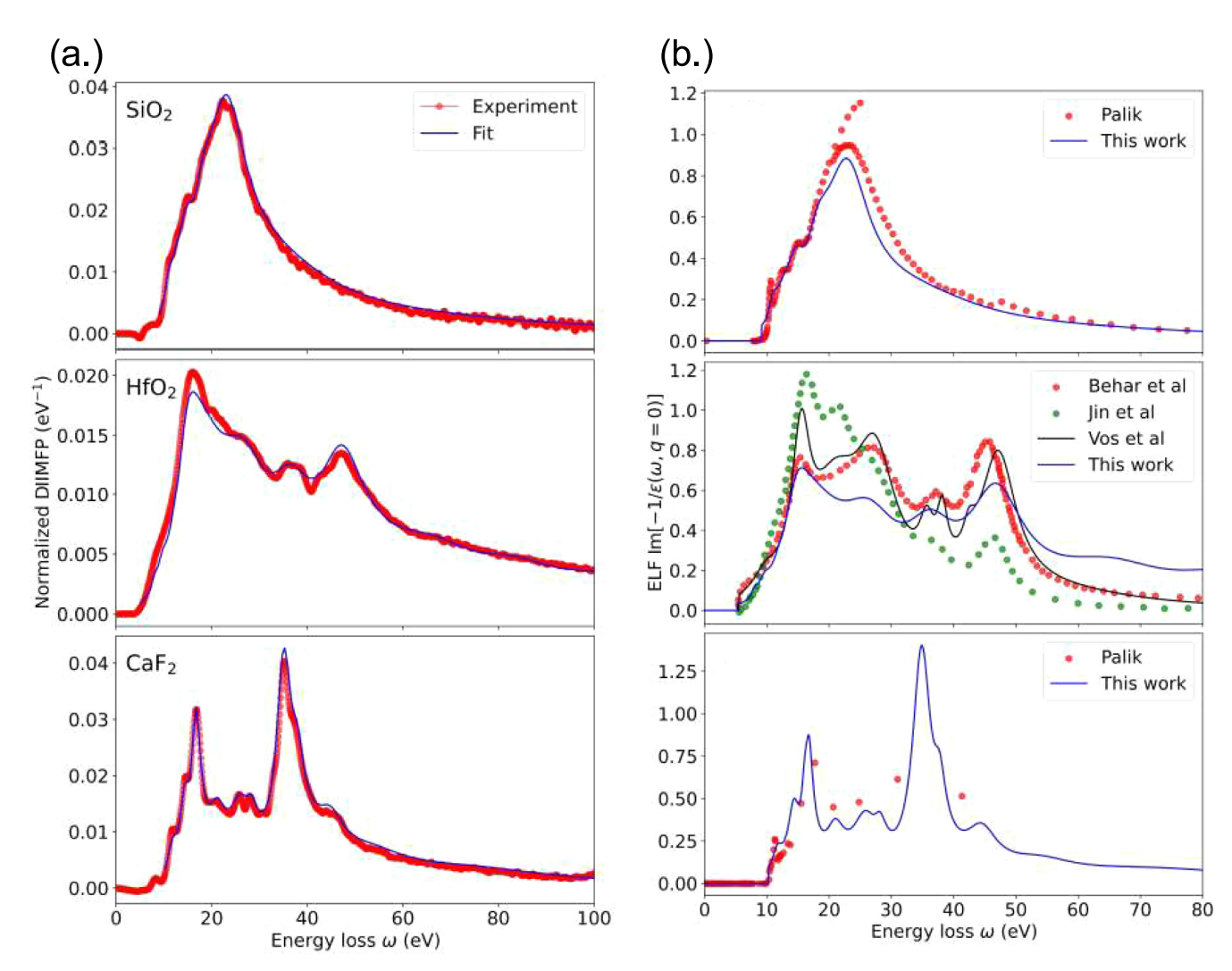


**FIGURE 3** | (a) Fit of the normalised DIIMFP data extracted from the measured REELS spectra using the Drude model dielectric function. (b) Comparison of the ELF derived from the REELS measurements (this work) with the ELFs derived from other measurements:  $SiO_2$  [22],  $HfO_2$  [29, 37, 38],  $CaF_2$  [24].

**TABLE 2** | Values of the atomic number Z,  $Z_{\text{eff}}$  from Equation (6), errors in the f-sum rule, values of  $P_{\text{eff}}$  from Equation (7) and errors in the KK-sum rule.

			f-sum rule	KK-sum rule		
Compound	$\boldsymbol{z}$	$Z_{ m eff}$	error (%)	$P_{ m eff}$	error (%)	
SiO <sub>2</sub>	30	29.19	-2.7	0.968	-3.2	
$\mathrm{HfO}_2$	88	86.84	-1.3	0.976	-2.3	
$CaF_2$	38	35.06	-7.7	0.99	-1.2	

TABLE 3 | Optimised oscillator parameters to model the Drude dielectric function defined in Equation (5).

SiO <sub>2</sub>			HfO <sub>2</sub>			CaF <sub>2</sub>		
$\overline{A_i}$	$\gamma_i$	$\omega_i$	$A_i$	$\gamma_i$	$\omega_i$	$A_i$	$\gamma_i$	$\omega_i$
18.16	1.50	10.58	17.29	1.36	7.75	29.50	1.93	11.25
25.94	2.78	12.13	42.74	2.08	9.11	56.38	2.39	13.39
39.79	3.51	13.72	65.83	2.80	10.96	21.35	1.53	15.57
42.60	3.92	16.90	49.92	4.06	12.67	2.11	1.00	16.53
91.29	8.53	20.61	107.58	12.84	17.63	27.84	3.51	20.53
134.48	30.18	35.17	124.10	12.39	24.93	70.38	5.17	25.08
186.26	79.87	69.21	102.81	9.46	34.92	12.13	2.28	27.87
			181.61	10.38	44.64	140.76	3.45	32.52
			208.15	22.98	64.65	8.65	2.23	37.43
			134.25	19.28	82.22	37.34	6.10	44.04
			206.31	24.59	102.23	40.77	13.20	53.85
			100.29	12.06	123.82	200.35	41.71	75.06

curves in the lower panels in Figure 1) with the energy loss function in the optical limit,  $\text{Im}\{-1/\epsilon(\omega,0)\}$  (black curves) shows that the REELS data are dominated by electron scattering with a small momentum transfer. The choice of  $\alpha=0.1$  then is justified [29, 39].

A comparison of the ELFs calculated using the oscillator parameters listed in Table 3 with the ELFs in the optical limit derived from different measurements found in the literature is shown in Figure 3b. In the case of  ${\rm SiO}_2$ , the ELF obtained in this work is in reasonable agreement with the ELF obtained by Kramers–Kronig analysis of reflectance data augmented by absorption measurements [22].

For HfO $_2$ , Jin et al. [38] derived the dielectric function employing the Drude–Lindhard model with no dispersion from REELS data taken at  $E_0=300$  eV and  $E_0=500$  eV. Behar et al. [37] obtained the same property from high-energy ( $E_0=20$  keV) transmission (TEELS) measurements performed by Frandon et al. [40] using the Mermin model with dispersion built-in (i.e.,  $\alpha=1.0$  is implicitly used in the Mermin loss function). More recently, Vos and Grande [29] derived the dielectric function from REELS measurements with the incident energies  $E_0=5$  keV and  $E_0=40$  keV which are close to those typically used in transmission EELS experiments. A value of 0.1 was assumed for  $\alpha$ . Vos

and Grande used the Tougaard-Chorkendorff deconvolution [6] to derive the NDIIMFP from the REELS spectra as well as the approach employed in the present work demonstrating a good overall agreement between the resulting NDIIMFPs (see Reference [29]).

Regarding CaF<sub>2</sub>, the only ELF data available for comparison were found in Reference [24] with sparse data in the XUV range but being in reasonable quantitative agreement with our experimental data.

The IMFP values for  ${\rm SiO}_2$ ,  ${\rm HfO}_2$  and  ${\rm CaF}_2$  as a function of the electron energy measured from the bottom of the conduction band were calculated using Equation (8) employing the Drude model dielectric function with oscillator parameters listed in Table 3. A value of  $\alpha=1$  was used for the IMFP calculations for meaningful comparison with the IMFP values obtained by other authors which assume a quadratic dispersion of the dielectric function (see also the discussion below). The resulting IMFPs for  ${\rm SiO}_2$ ,  ${\rm HfO}_2$  and  ${\rm CaF}_2$  are shown in Figure 3c. The IMFPs calculated in the present work for all three compounds are seen to be consistent with the IMFPs calculated using the relativistic TPP-2M formula given by Equation 12 in Reference [28]. The parameters for this formula were calculated using Equations (15a–15e) from Reference [28] with

the values of the band gap  $E_{\rm g}$  and the mass density  $\rho$  listed in Table 1; the values of the plasmon energy were estimated as  $E_p=28.816\sqrt{N_{\rm v}\rho/M}$  (see Table 1). The average RMS difference between the IMFPs calculated in this work and the IMFPs calculated using the TPP-2M formula for SiO<sub>2</sub>, HfO<sub>2</sub> and CaF<sub>2</sub> is 22%, 16% and 23 %, respectively, for the energy

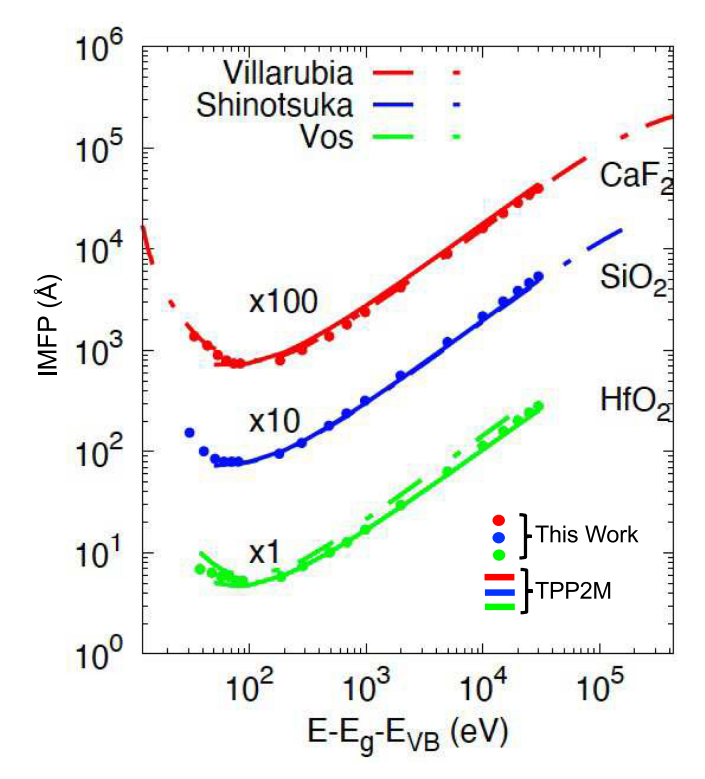


**FIGURE 4** | Comparison of the IMFP calculated using the energy loss function derived from the REELS measurements (this work, filled circles) with the data obtained by other authors (dash-dotted curves): SiO<sub>2</sub> [28], HfO<sub>2</sub> [29], CaF<sub>2</sub> [3]. The TPP-2M IMFP values were calculated using Equation (12) from Reference [28]. (solid curves).

range between 200–30000 eV. The lower limit of this energy range is due to the TPP-2M equation being less reliable for energies under 200 eV [28].

The IMFP data for  $SiO_2$  and  $CaF_2$  in Figure 3c are also compared with those reported by Shinotsuka et al. [28] and Flores-Mancera et al. [3], respectively, demonstrating a reasonable agreement. Regarding  $HfO_2$ , the IMFP values calculated in this work were compared with the IMFP values (green solid curve in Figure 3c) computed using Equation (8) employing the Drude–Lindhard model dielectric function with the oscillator parameters listed in Table 1 of Reference [29], exhibiting reasonable agreement with a 12% RMS-difference over the energy range between 50–30000 eV.

At this stage, the treatment of the dispersion in the framework of inelastic electron scattering deserves to be discussed in some detail. This concerns the value of the dispersion constant  $\alpha$  used in (1) evaluation of the DIIMFP in the procedure to extract optical constants and (2) the value of the dispersion constant used in evaluating the IMFP. In the present work, a value of  $\alpha=0.1$  was used throughout in the fitting of the normalised DIIMFP. In addition, the fitting has also been carried out using  $\alpha$  as an additional fit parameter, resulting in small values for  $\alpha\sim0.05-0.1$ . Similar results were obtained earlier for a number of organic insulators [8, 11]. In the case of metals, however, a value close to unity always represents a reasonable choice [20].

Furthermore, and most importantly, when evaluating the IMFP, the use of a value of  $\alpha$  close to zero underestimates IMFP values by a factor of two or more [8]. Similar results were obtained in the present work for the IMFP using Equation (8) (not shown): For  $\alpha \sim 0$ , the IMFP values are a factor of 2–3 below the values shown in Figure 4. The fact that the correct IMFP values are obtained by using  $\alpha \sim 1$  in Equation (8) was proven by comparing IMFP values derived from EPES [8] with values obtained from

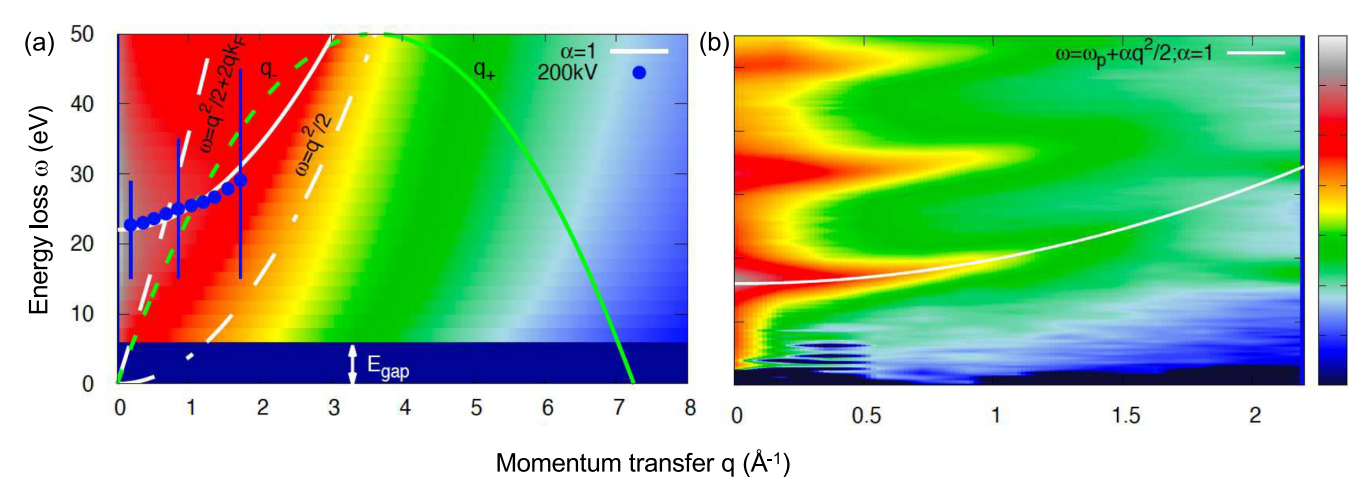


**FIGURE 5** | (a) The energy loss function of the dielectric function for PMMA calculated based on the Drude model using the oscillator parameters from [21] is shown on a false colour scale on the complex  $(q, \omega)$ -plane; the blue circles are the experimental results for the dispersion as determined by energy loss measurements in transmission, the error bars indicate the width of the plasmon. The solid curve illustrates the dispersion according to Equation 1 with  $\alpha = 1$ . The white dashed dotted line is the Bethe-ridge  $E \sim q^2/2$ ; the dashed white lines indicate the lower limit of the Compton profile, (the electron-hole pair continuum), that is, the function  $E = q^2/2 + 2qk_F$ , where  $k_F$  is the Fermi wave vector; the green dashed  $(q_-)$  and solid  $(q_+)$  curves describe the limits of integration (Equation 4) of the momentum transfer in the evaluation of the DIIMFP as per Equation 3, for a primary energy of  $E_0 = 50$  eV. (b) Raw experimental energy loss spectra of aluminium shown on a false colour scale.

linear response theory and optical data in which  $\alpha$  is set to unity. These latter two approaches give excellent mutual agreement for organic insulators [8]. In this connection, it is important to note that the only parameter needed for analysis of EPES is the differential *elastic* scattering cross-section [41, 42]; the dispersion of loss features does not play any role in the analysis of EPESdata to determine the IMFP. It is also important to realise in this connection that while the electrons making up the elastic peak are coming from the very surface of the solid, the intensity of the elastic peak is determined by those electrons that are not elastically scattered, that is, those that wind up in the inelastic background in a REELS spectrum. Obviously, the inelastic background corresponds to scattering processes taking place deeper inside the volume of the material. In other words, EPES intensities provide a measure of the IMFP inside the volume of the surface. On the other hand, the part of the REELS spectrum used to extract optical constants is the single scattering contribution which predominantly corresponds to an inelastic process taking place very close to the surface (typically at depths less than the IMFP for any given incidence and emission angle).

A measurement of the dispersion of the plasmon in polymethylmethacrylate (PMMA) and Aluminium is presented in Figure 5. The white solid curves indicate a quadratic dispersion, which is directly confirmed by the raw data for Al in Figure 5b. The blue data points in Figure 5a represent the plasmon dispersion in PMMA, which are also seen to follow a quadratic dispersion. The error bars in the blue data points give an impression of the width of the plasmon for a given momentum transfer q. For values beyond  $q \sim 1\text{Å}^{-1}$ , the plasmon width becomes excessively large, indicating strong damping, both for Al and for PMMA. This is expected since for a momentum transfer exceeding the Fermi wavevector (with a typical value around  $k_F \sim 1\text{\AA}^{-1}$ ), the electron-hole pair continuum is reached; that is, the plasmon oscillation, essentially a collective excitation brought about in a distant collision (small q), is no longer sustained and the regime of direct knock-on collisions leading to electron-hole pair excitation is reached for large momentum transfers. The latter regime coincides with the electron-Compton profile  $\omega = q^2/2 \pm 2qk_F$  around the Bethe-ridge  $\omega = q^2/2$ , which dictate energy and momentum conservation in the scattering process. The plasmon dispersion slowly converges towards the Betheridge for large energy losses.

The green dashed and solid curves indicate the minimum and maximum momentum transfer in an inelastic collision (see Equation 4) for a 50 eV primary electron. The plasmon dispersion intersects the (dashed)  $q_-$ -curve but does not extend beyond the Bethe-ridge, also for higher primary energies. The above implies that the integrand in Equation (3) under the  $q_+$ -curve is always small. This changes dramatically when a value of  $\alpha=0$  is used in evaluating the IMFP. In this case, the plasmon loss contributes to the integrand both under the  $q_-$ - and  $q_+$ -curves, leading to a much larger value of the integrand under the  $q_+$ -curve. Consequently, a smaller value for the IMFP would result. However, such a procedure would also imply violation of energy and momentum conservation in the collision.

From the above considerations, it must be concluded that a quadratic dispersion governs the scattering process but that small momentum transfer inelastic processes dominate in a REELS

spectrum in the case of insulators, consistent with a retrieved value of  $\alpha \sim 0$  in the analysis of REELS data. In metals, the commonly made assumption that all possible momentum transfers contribute to the inelastic processes in a REELS spectrum is confirmed. While we have no conclusive answer to the question why the kinematics in REELS are different for conducting and insulating materials, we note that the character of the collective excitations can be more "plasmonic" or more "excitonic" depending on the extent of localisation of the involved states [43, 44], but the influence on the kinematically allowed (or prefered) transitions has not been worked out for electron backscattering experiments.

In practice, the above suggests that for analysis of REELS spectra, it is recommendable to treat  $\alpha$  as a fit parameter or, alternatively, use a vanishing value for insulators and  $\alpha=1$  for conductors. For evaluating the IMFP using optical constants,  $\alpha$  should always be taken to be unity.

# 5 | Summary

Normalised DIIMFPs were derived in absolute units from electron energy loss spectra acquired in reflection mode (REELS) for three inorganic compounds SiO2, HfO2 and CaF2 employing the deconvolution procedure of Refs. [5, 36, 45]. The optical constants were obtained by fitting the normalised DIIMFPs with a set of oscillator parameters using the extended Drude model dielectric function [31] assuming a weak q- dependence introduced by a quadratic dispersion of the dielectric function with  $\alpha = 0.1$  in Equation (1). The resulting energy loss functions (ELF) calculated based on these oscillator parameters were compared with the ELFs found in the literature (SiO<sub>2</sub> [22], HfO<sub>2</sub> [29, 37, 38], CaF<sub>2</sub> [24]) demonstrating an acceptable agreement. The inelastic mean-free paths (IMFP) were calculated based on the optical constants obtained in this work assuming a full quadratic dispersion of the dielectric function with  $\alpha = 1$  in Equation (1). The resulting IMFP values were found to be in satisfactory agreement with those calculated employing the relativistic TPP-2M formula [28] as well as the results reported by other authors [3, 28, 29].

In practice, the above suggests that for analysis of REELS spectra, it is recommendable to treat  $\alpha$  as a fit parameter or, alternatively, use a vanishing value for insulators and  $\alpha=1$  for conductors. For evaluating the IMFP using optical constants,  $\alpha$  should always be taken to be unity.

# Acknowledgements

The computational results presented have been achieved using the Vienna Scientific Cluster (VSC). The authors acknowledge TU Wien Bibliothek for financial support through its Open Access Funding Programme. Open access funding provided by Technische Universitat Wien/KEMÖ. [Correction added on 30 April 2025, after first online publication: Projekt KEMÖ funding statement has been added.]

### References

1. W. Banerjee, A. Kashir, and S. Kamba, "Hafnium Oxide  $(HfO_2)$  – A Multifunctional Oxide: A Review on the Prospect and Challenges of Hafnium Oxide in Resistive Switching and Ferroelectric Memories," *Small* 18 (2022): 2107575, https://doi.org/10.1002/smll.202107575.

- 2. V. Valković, *Radioactivity in the Environment*, ed. V. Valković (Elsevier Science, 2000), 117–258, https://www.sciencedirect.com/science/article/pii/B9780444829542500058.
- 3. M. A. Flores-Mancera, J. S. Villarrubia, and G. Massillon-JL, "Electron Inelastic Mean Free Paths for LiF, CaF2, Al2O3, and Liquid Water from 433 keV down to the Energy Gap," *ACS Omega* 5 (2020): 4139–4147, https://doi.org/10.1021/acsomega.9b03872.
- 4. R. Ropp, *Encyclopedia of the Alkaline Earth Compounds*, ed. R. Ropp (Elsevier, 2013), 25–104, https://www.sciencedirect.com/science/article/pii/B9780444595508000028.
- 5. W. S. M. Werner, "Simple Algorithm for Quantitative Analysis of Reflection Electron Energy Loss Spectra (REELS)," *Surface Science* 604 (2010): 290.
- 6. S. Tougaard and I. Chorkendorff, "Differential Inelastic Electron Scattering Cross Sections From Experimental Reflection Electron-Energy-Loss Spectra: Application to Background Removal in Electron Spectroscopy," *Physical Review B* 35 (1987): 6570.
- 7. S. Hajati, O. Romanyuk, J. Zemek, and S. Tougaard, "Validity of Yubero-Tougaard Theory to Quantitatively Determine the Dielectric Properties of Surface Nanofilms," *Physical Review B* 77 (2008): 155403.
- 8. W. S. M. Werner, F. Helmberger, M. Schürrer, O. Ridzel, M. Stöger-Pollach, and C. Eisenmenger-Sittner, "Electron Inelastic Mean Free Path (IMFP) Values of Kapton, Polyethylene (PE), Polymethylmethacrylate (PMMA), Polystyrene (PS) and Polytetrafluoroethylene (PTFE) Measured With Elastic Peak Electron Spectroscopy (EPES)," Surface and Interface Analysis 54 (2022): 855–863, https://doi.org/10.1002/sia.7098.
- 9. M. Vos, "A Model Dielectric Function for Low and Very High Momentum Transfer," *Nuclear Instruments and Methods in Physics Research, Section B: Beam Interactions with Materials and Atoms* 366 (2016): 6–12, https://doi.org/10.1016/j.nimb.2015.09.091.
- 10. H. Shinotsuka, S. Tanuma, and C. J. Powell, "Calculations of Electron Inelastic Mean Free Paths. XIII. Data for 14 Organic Compounds and Water Over the 50 eV to 200 keV Range With the Relativistic Full Penn Algorithm," *Surface and Interface Analysis* 54, no. 5 (2022): 534–560.
- 11. O. Y. Ridzel, H. Kalbe, V. Astašauskas, P. Kuksa, A. Bellissimo, and W. S. M. Werner, "Optical Constants of Organic Insulators in the UV Range Extracted From Reflection Electron Energy Loss Spectra," *Surface and Interface Analysis* 54 (2022): 487–500.
- 12. W. S. Werner, F. Helmberger, M. Schürrer, O. Ridzel, M. Stöger-Pollach, and C. Eisenmenger-Sittner, "Electron Inelastic Mean Free Path (IMFP) Values of Kapton, Polyethylene (PE), Polymethylmethacrylate (PMMA), Polystyrene (PS) and Polytetrafluoroethylene (PTFE) Measured With Elastic Peak Electron Spectroscopy (EPES)," *Surface and Interface Analysis* 54 (2022): 855–863.
- 13. V. Astašauskas, A. Bellissimo, P. Kuksa, C. Tomastik, H. Kalbe, and W. S. Werner, "Optical and Electronic Properties of Amorphous Silicon Dioxide by Single and Double Electron Spectroscopy," *Journal of Electron Spectroscopy and Related Phenomena* 241 (2020): 146829, https://linkinghub.elsevier.com/retrieve/pii/S0368204818301993.
- 14. W. S. M. Werner, W. Smekal, C. Tomastik, and H. Störi, "Surface Excitation Probability of Medium Energy Electrons in Metals and Semi-conductors," *Surface Science* 486 (2001): L461–L466, https://www.sciencedirect.com/science/article/pii/S0039602801010913.
- 15. E. D. Palik,  $Handbook\ of\ Optical\ Constants\ of\ Solids\ (Academic\ Press, 1985).$
- 16. E. D. Palik, Handbook of Optical Constants of Solids I& II (Academic Press, 1985, 1991).
- 17. D. W. Lynch and W. R. Hunter, *Handbook of Optical Constants of Solids II*, vol. I (Academic Press, 1991), chap. 2.1.III.

- 18. D. Y. Smith, Handbook of Optical Constants of Solids I& II, Chap. 3, vol. I of [20] (1985, 1991).
- 19. R. Egerton, *Electron Energy-Loss Spectroscopy in the Electron Microscope* (Springer, 2011), https://doi.org/10.1007/978-1-4419-9583-4.
- 20. W. S. M. Werner, C. Ambrosch-Draxl, and K. Glantschnig, "Optical Constants and Inelastic Electron-Scattering Data for 17 Elemental Metals," *Journal of Physical and Chemical Reference Data* 38, no. 4 (2009): 1013–1092.
- 21. O. Y. Ridzel, H. Kalbe, V. Astašauskas, P. Kuksa, A. Bellissimo, and W. S. M. Werner, (2022).
- 22. H. Philipp, *Handbook of Optical Constants of Solids*, ed. E. D. Palik (Academic Press, 1985), 749–763, https://www.sciencedirect.com/science/article/pii/B978008054721350040X.
- 23. M. Couillard, M. Kociak, O. Stéphan, G. A. Botton, and C. Colliex, "Multiple-Interface Coupling Effects in Local Electron-Energy-Loss Measurements of Band Gap Energies," *Physical Review B* 76 (2007): 165131.
- 24. D. Bezuidenhout, *Handbook of Optical Constants of Solids*, ed. E. D. Palik (Academic Press, 1998), 815–835, https://www.sciencedirect.com/science/article/pii/B9780080556307500511.
- 25. C. T. H. S. W. S. M. Werner and W. Smekal, *Surface Science* 486 (2001): L461–L466.
- 26. D. R. Lide, ed., CRC Handbook of Chemistry and Physics, 88th ed. (CRC press, 2008).
- 27. W. Werner, W. Smekal, C. Powell, and J. Gorham, "Simulation of Electron Spectra for Surface Analysis (SESSA)Version 2.2 User's Guide," (2021), https://tsapps.nist.gov/publication/get\_pdf.cfm?pub\_id=931745.
- 28. H. Shinotsuka, S. Tanuma, C. J. Powell, and D. R. Penn, "Calculations of Electron Inelastic Mean Free Paths. XII. Data for 42 Inorganic Compounds Over the 50 eV to 200 keV Range With the Full Penn Algorithm," *Surface and Interface Analysis* 51 (2019): 427–457, https://doi.org/10.1002/sia.6598.
- 29. M. Vos and P. L. Grande, "The Relation Between the Electron Energy Loss Spectra of Hafnia and Its Dielectric Function," *Surface Science* 630 (2014): 1–8, https://doi.org/10.1016/j.susc.2014.06.008.
- 30. M. Scrocco, "Satellites in X-ray Photoelectron Spectroscopy of Insulators. I. Multielectron Excitations in CaF 2, SrF 2, and BaF 2," *Physical Review B* 32 (1985): 1301, https://doi.org/10.1103/PhysRevB. 32.1301.
- 31. M. Vos and P. L. Grande, "Extracting the Dielectric Function From High-Energy REELS Measurements," *Surface and Interface Analysis* 49 (2017): 809–821, https://doi.org/10.1002/sia.6227.
- 32. S. G. Johnson, "The NLOPT Nonlinear-Optimization Package," http://github.com/stevengj/nlopt.
- 33. A. R. Conn, N. I. M. Gould, and P. Toint, "A Globally Convergent Augmented Lagrangian Algorithm for Optimization With General Constraints and Simple Bounds," *SIAM Journal on Numerical Analysis* 28 (1991): 545–572, https://doi.org/10.1137/0728030.
- 34. E. Birgin and J. Martínez, "Improving Ultimate Convergence of an Augmented Lagrangian Method," *Optimization Methods and Software* 23 (2008): 177–195, https://doi.org/10.1080/10556780701577730.
- 35. M. J. D. Powell, A Direct Search Optimization Method That Models the Objective and Constraint Functions by Linear Interpolation (Springer, 1994), 51–67, https://doi.org/10.1007/978-94-015-8330-5\_4.
- 36. S. Hummel, A. Gross, and W. S. M. Werner, "Richardson-Lucy Deconvolution of Reflection Electron Energy Loss Spectra," *Surface and Interface Analysis* 41 (2009): 357–360.
- 37. M. Behar, R. C. Fadanelli, I. Abril, et al., "Energy Loss of Proton,  $\alpha$  Particle, and Electron Beams in Hafnium Dioxide Films," *Physical Review A: Atomic, Molecular, and Optical Physics* 80 (2009): 062901, https://doi.org/10.1103/PhysRevA.80.062901.

- 38. H. Jin, S. K. Oh, H. J. Kang, and S. Tougaard, "Electronic Properties of Ultrathin HfO2, Al2O3, and Hf–Al–O Dielectric Films on Si (100) Studied by Quantitative Analysis of Reflection Electron Energy loss Spectra," *Journal of Applied Physics* 100 (2006): 083713, https://doi.org/10.1063/1.2360382.
- 39. W. S. Werner, F. Helmberger, M. Schürrer, C. Eisenmenger-Sittner, and O. Y. Ridzel, "Measurement of the Surface Excitation Parameter of Kapton, Polyethylene (PE), Polymethyl Methacrylate (PMMA), Polystyrene (PS) and Polytetrafluoroethylene (PTFE)," *Surface and Interface Analysis* 54, no. 7 (2022): 681–687, https://doi.org/10.1002/sia.7080.
- 40. J. Frandon, B. Brousseau, and F. Pradal, "Electronic Excitations in Some Transition Metals and Their Oxides. Characteristic Energy Loss Measurements up to 50 eV," *Physica Status Solidi B* 98 (1980): 379–385, https://doi.org/10.1002/pssb.2220980140.
- 41. F. Salvat, A. Jablonski, and C. J. Powell, "ELSEPA—Dirac Partial-Wave Calculation of Elastic Scattering of Electrons and Positrons by Atoms, Positive Ions and Molecules," *Computer Physics Communications* 165 (2005): 157–190.
- 42. A. Jabłonski, F. Salvat, and C. J. Powell, "Comparison of Electron Elastic-Scattering Cross Sections Calculated From Two Commonly Used Atomic Potentials," *Journal of Physical and Chemical Reference Data* 33 (2004): 409–451.
- 43. C. Horie, "Exciton and Plasmon in Insulating Crystals," *Progress of Theoretical Physics* 21 (1959): 113–134.
- 44. I. Egri, "Excitons and Plasmons in Metals, Semiconductors and Insulators: A Unified Approach," *Physics Reports* 119, no. 6 (1985): 363–402.
- 45. W. S. M. Werner, K. Glantschnig, and C. Ambrosch-Draxl, "Optical Constants and Inelastic Electron-Scattering Data for 17 Elemental Metals," *Journal of Physical and Chemical Reference Data* 38 (2009): 1013–1092, https://doi.org/10.1063/1.3243762.